Combustion and Flame 161 (2014) 2815–2824

Contents lists available at ScienceDirect

Combustion and Flame

journal homepage: www.elsevier.com/locate/combustflame

Radiation-induced uncertainty in laminar flame speed measured from propagating spherical flames

Hao Yu [a], Wang Han [a], Jeffrey Santner [b], Xiaolong Gou [c], Chae Hoon Sohn [d], Yiguang Ju [b], Zheng Chen [a,c,*]

[a] SKLTCS, Department of Mechanics and Engineering Science, College of Engineering, Peking University, Beijing 100871, China
[b] Department of Mechanical and Aerospace Engineering, Princeton University, Princeton, NJ 08544, USA
[c] Key Laboratory of Low-grade Energy Utilization Technologies and Systems, School of Power Engineering, Chongqing University, Chongqing 400044, China
[d] Department of Mechanical Engineering, Sejong University, Seoul 143-747, Republic of Korea

ARTICLE INFO

Article history:
Received 26 February 2014
Received in revised form 15 April 2014
Accepted 13 May 2014
Available online 6 June 2014

Keywords:
Radiation
Uncertainty
Laminar flame speed
Propagating spherical flame
Elevated temperature and pressure

ABSTRACT

Laminar flame speeds measured using the propagating spherical flame method are inherently affected by radiation. Under certain conditions, a substantial uncertainty in laminar flame speed measurement is caused by radiation, which results in a great concern for kinetic mechanism validation and development. In this study, numerical simulations with detailed chemistry and different radiation models are conducted to examine the effects of radiation on spherical flame propagation. The emphasis is placed on quantifying the uncertainty and corrections associated with radiation in laminar flame speed measurements using propagating spherical flames. The radiation effects on flame speeds at normal and elevated temperatures and pressures are examined for different fuel/air mixtures including methane, propane, isooctane, syngas, hydrogen, dimethyl ether, and n-heptane. The radiative effects are conservatively evaluated without considering radation reflection on the wall. It is found that radiation-induced uncertainty in laminar flame speeds is affected in the opposite ways by the initial temperature and pressure. An empirical correlation quantifying the uncertainty associated with radiation is obtained. This correlation is shown to work for different fuels at normal and elevated temperatures and pressures. Therefore, it can be directly used in spherical flame experiments measuring the laminar flame speed. Furthermore, a method to obtain the radiation-corrected flame speed (RCFS) is presented and it can be used for laminar flame speed measurement using the propagating spherical flame method.

1. Introduction

The laminar flame speed, S_u^0, is defined as the speed at which a planar, unstretched, adiabatic, premixed flame propagates relative to the unburned gas. It is one of the most important parameters of a combustible mixture. Accurate determination of S_u^0 is important for developing and validating chemical mechanisms and surrogate fuel models [1–4], especially at high pressure [5]. Predictions of S_u^0 can be easily obtained through simulating one-dimensional, planar, adiabatic, premixed flames (e.g. using PREMIX code) with chemical models. However, in experiments it is very difficult to establish a planar, unstretched, adiabatic flame and different flame configurations (such as outwardly propagating spherical flame, counterflow or stagnation flame, and Bunsen flame) have been used to measure S_u^0. Different effects such as stretch, flow compression, and heat loss must be subtracted from the experimental data in order to unambiguously determine S_u^0. Several experimental approaches have been developed to measure S_u^0. Currently, due to the simple flame configuration and well-defined stretch rate, the propagating spherical flame method is popularly used to measure S_u^0 (e.g., [6–15]). In this method, a quiescent homogeneous premixture in a closed chamber is ignited at the center and the ignition kernel evolves into an outwardly propagating spherical flame. The flame front history, $R_f = R_f(t)$, is recorded by using high-speed schlieren or shadowgraphy. Usually the stretched flame speed relative to burned gas, S_b, is first obtained from flame front history and extrapolated to zero stretch rate to get the unstretched laminar flame speed, S_b^0, relative to burned gas. Then $S_u{}^0$ can be determined through $S_u^0 = \sigma S_b^0$, where $\sigma = \rho_b/\rho_u$ is the density ratio between the burned gas (at adiabatic equilibrium condition) and unburned gas [6–15].

However, there still exist considerable discrepancies in the laminar flame speeds measured by different researchers using propagating spherical flames at the same conditions – sometimes

* Corresponding author at: SKLTCS, Department of Mechanics and Engineering Science, College of Engineering, Peking University, Beijing 100871, China.
E-mail address: cz@pku.edu.cn (Z. Chen).

http://dx.doi.org/10.1016/j.combustflame.2014.05.012
0010-2180/

exceeding typical quoted uncertainties in the measurements [4,16,17]. Therefore, substantial attention has been devoted to obtaining accurate S_u^0 from propagating spherical flames. For examples, the effects of ignition and unsteady transition [18–20], buoyancy [21], flow compression and finite chamber confinement [22,23], flame instability [24], and nonlinear extrapolation [25–28] have been examined recently.

Radiation is another process which can significantly modify the flame propagation speed and limits via radiation heat loss and radiation absorption [29–31]. In spherical flame experiment, radiation of H_2O and CO_2 in the burned gas region cannot be avoided and affects the speed of flame propagation. Therefore, all laminar flame speed data measured using the propagating spherical flame method are inherently affected by radiation. However, radiation effects are usually neglected in experiments [6–15]. In fact, it is difficult to quantify the correction in S_u^0 associated with radiation due to its nonlinear character, though in the literature there are many theoretical studies (e.g., [32–35]) investigating radiation effects on spherical flame propagation. Recently, radiation effects on laminar flame speed measurement using the propagating spherical flame method have drawn attention from researchers. Taylor and coworkers [6,36] first analyzed the flame speed measurement error in spherical flames due to thermal radiation and found that the radiation-induced reduction in S_u^0 is less than 5% under worst-case conditions. Chen et al. [37] and Qiao et al. [38] assessed radiation (re)absorption effects on spherical flame propagation and concluded that quantitative prediction of flame speed of CO_2 diluted mixtures requires an accurate spectral dependent radiation model. Chen [39] studied radiation effects on methane/air flames near the lean flammability limit. It was found that radiation reduces the flame temperature and induces inward flow of burned gas, both of which slow down the flame propagation. Radiation was shown to cause up to 25% under-prediction of S_u^0. Beeckmann et al. [40] and Jayachandran et al. [41] found that radiation cannot be neglected even for mixtures not close to the flammability limits. Santner et al. [42] conducted a semi-analytical investigation of radiation heat loss on the uncertainty of S_u^0 measured at high pressure. They demonstrated that the high pressure flame speeds of H_2/He/O_2 are only slightly affected by radiation.

Since uncertainty quantification for laminar flame speed measured in experiments is crucial to kinetic model development and optimization [44,45], accurate determination of uncertainty in S_u^0 associated with radiation is very important [42]. However, in studies [36–42] mentioned above, radiation-induced uncertainty in S_u^0 was not quantitatively assessed or was assessed only for certain types of fuel/air mixtures. There is no general correlation for radiation-induced uncertainty in S_u^0 which can be directly used in laminar flame speed measurements by the propagating spherical flame method. Therefore, the first objective of this study is to provide a general quantification of the uncertainty in S_u^0 associated with radiation for different fuel/air mixtures.

Except the work of Ju and coworkers [37,42] and Jayachandran et al. [41] which considered radiation effects at elevated pressures, the previous studies were all focused on spherical flames at normal temperature and pressure (NTP). It is not clear how the initial temperature and pressure affect radiation-induced uncertainty in S_u^0 measured from propagating spherical flames. Therefore, the second objective is to evaluate the radiation effects at elevated temperature and pressure and to find the change of radiation-induced uncertainty in S_u^0 with the initial temperature and pressure.

In kinetic model validation and optimization, usually the predicted adiabatic laminar flame speeds are used. To compare results predicted by kinetic models with those from measurements using propagating spherical flames, radiation-correction must be conducted to account for a decrease in laminar flame speed due to radiative loss. The third objective of this study is therefore to get the radiation-corrected flame speed (RCFS).

Based on the objectives discussed above, direct numerical simulations are conducted to examine the effects of radiation on spherical flame propagation and to quantify uncertainty and corrections associated with radiation in laminar flame speed measurement for different fuels in air at a variety of temperatures, pressures, and equivalence ratios. An empirical correlation for uncertainty in S_u^0 associated with radiation is obtained. It works for different fuels at normal and elevated temperatures and pressures and can be directly used in laminar flame speed measurements using the propagating spherical flame method.

The paper is organized as follows: in Section 2, numerical methods and specifications are presented; then, in Section 3, radiation effects on spherical flame propagation are briefly described; radiation-induced uncertainty/reduction in laminar flame speed measurement are quantified in Section 4, based on which the method to get RCFS is proposed in Section 5; and finally, the conclusions are summarized in Section 6.

2. Numerical methods and specifications

One-dimensional outwardly propagating spherical flames are simulated using the in-house code for Adaptive Simulation of Unsteady Reacting Flows (A-SURF) [19,39]. The conservation equations for a multi-species reactive flow are solved by using the finite volume method [19,39]. The CHEMKIN packages [46] are incorporated into A-SURF to calculate the temperature- and component-dependent thermodynamic and transport properties. A-SURF has been successfully used in previous studies on ignition and spherical flame propagation (e.g., [47–51]). The details on governing equations, numerical schemes, and code validation can be found in [19,39].

Three radiation models are employed so that the radiation effects can be quantified through comparison between results predicted by different models. These models are summarized in Table 1: the first one is the adiabatic model (denoted by 'ADI') in which radiation is neglected; the second one is the optically thin model (denoted by 'OTM') in which only radiation emission from CO_2, H_2O, CO, and CH_4 is considered [29]; and the third one is the statistical narrow band model (denoted by 'SNB') in which a fitted statistical narrow-band correlated-k (FSNB-CK) method [37] is employed to calculate radiative transport including both emission and re-absorption. The Planck mean coefficients in the OTM model were derived from the SNB model in the optically thin limit [29]. Detailed validation of the SNB model for H_2O and CO_2 radiation can be found in [43]. It was shown in Ref. [37] that the SNB model reproduces the theoretical radiation flux at hollow sphere boundaries and the measured flame speed. However, the OTM under-predicts the flame speed since radiation loss is over-predicted. The drawback of the OTM is that it over-predicts the radiative loss and is less accurate than the SNB model. The disadvantage of the SNB model is that it takes much more computational time than the OTM.

We consider several types of fuel: methane, propane, iso-octane, syngas (with five different H_2/CO ratios: 5/95, 10/90, 25/75, 50/50, and 100/0), dimethyl ether (DME), and n-heptane.

Table 1
Three models for radiation.

Abbreviation	Model description
ADI	Adiabatic model without radiative loss
OTM	Optically thin model; only radiative emission is considered
SNB	Statistical narrow band model; radiative emission and absorption are considered

Table 2
Summary of fuel/air mixtures and conditions.

No.	Fuel	T_u (K)	P	ϕ	Radiation model
1	CH_4	298	1 atm	0.55, 0.6, 0.7 …1.4	ADI, OTM, SNB
2	C_3H_8	300	1 atm	0.65, 0.7, 0.8 …1.7	ADI, OTM, SNB
3	iC_8H_{18}	298	1 atm	0.7, 0.8 …1.6	ADI, OTM, SNB
4	H_2/CO = 5/95	298	1 atm	0.8, 1, 2, 3, 4, 5	ADI, OTM, SNB
5	H_2/CO = 10/90	298	1 atm	0.8, 1, 2, 3, 4, 5	ADI, OTM, SNB
6	H_2/CO = 25/75	298	1 atm	0.8, 1, 2, 3, 4, 5	ADI, OTM, SNB
7	H_2/CO = 50/50	298	1 atm	0.8, 1, 2, 3, 4, 5	ADI, OTM, SNB
8	H_2/CO = 100/0	298	1 atm	0.8, 1, 2, 3, 4, 5	ADI, OTM, SNB
9	CH_3OCH_3	298	1 atm	0.6, 0.7 …1.7	ADI, SNB
10	nC_7H_{16}	298	1 atm	0.7, 0.8 …1.45, 1.5	ADI, SNB
11	CH_4	373	1 atm	0.55, 0.6, 0.7 …1.4	ADI, SNB
12	CH_4	450	1 atm	0.55, 0.6, 0.7 …1.4	ADI, SNB
13	iC_8H_{18}	358	0.1 MPa	0.7, 0.8 …1.6	ADI, SNB
14	iC_8H_{18}	418	0.1 MPa	0.7, 0.8 …1.6	ADI, SNB
15	CH_4	373	5 atm	0.6, 0.7 …1.4	ADI, SNB
16	CH_4	450	5 atm	0.6, 0.7 …1.4	ADI, SNB
17	CH_4	450	10 atm	0.6, 0.7 …1.4	ADI, SNB
18	iC_8H_{18}	418	0.5 MPa	0.7, 0.8 …1.6	ADI, SNB
19	CH_4	298	1, 2, 4, 8, 12 atm	1.0	ADI, SNB
20	CH_4	373	1, 2, 4, 8, 12 atm	1.0	ADI, SNB
21	CH_4	450	1, 2, 4, 8, 12 atm	1.0	ADI, SNB

Table 2 summarizes the mixtures and conditions (in terms of initial temperature, T_u, pressure, P, and equivalence ratio, ϕ) considered in simulation. There are 21 sets of mixtures and conditions: Nos. 1–10 correspond to fuel/air mixtures at NTP; Nos. 11–14 correspond to mixtures at elevated temperature and atmospheric pressure; and Nos. 15–21 are mixtures at elevated temperature and pressure. The radiation models, ADI and SNB, are used for all these 21 sets; while OTM is considered only for Nos. 1–8. In total, 408 propagating spherical flames are simulated using A-SURF. In simulations, detailed chemistry is considered: GRI-Mech 3.0 [52] for methane, the mechanism of Qin et al. [53] for propane, the high-temperature mechanism of Chaos et al. [54] for iso-octane and n-heptane, the mechanism of Davis et al. [55] for syngas, and the mechanism of Zhao et al. [56] for DME. Detailed chemistry is efficiently handled in A-SURF with the help of algorithms introduced in [57,58].

The computational domain is $0 \leqslant r \leqslant R_W$, where R_W is the chamber radius. A large value of R_W = 50 or 100 cm is used in simulation, so that the effects of pressure rise and wall confinement [22,23,39] on spherical flame propagation can be neglected. We also conduct simulations for some mixtures with smaller computational domain of R_W = 10 and 7.5 cm. It is found that the size of computational domain has little effect on the value of relative reduction in unstretched laminar flame speed caused by radiation. Zero flow speed and zero gradients of temperature and mass fractions are enforced at the center (r = 0) and wall ($r = R_W$) boundaries. The wall is considered as a black body without radiation reflection. In real experiments the radiation reflects from the walls and is re-absorbed by the products, which reduces the radiative heat losses. However, in practical experiments, the ratio between the flame radius and inner wall radius is usually within 0.2–0.3, indicating that very small amount of wall-reflected radiation is absorbed by the burned gas inside the spherical flame. Nevertheless, the radiative effects are conservatively evaluated in the present study without considering wall-reflected radiation. The spherical flame is initiated at the center by a small hot kernel (its radius is around 1–2 mm) of the burned product of the static fresh mixture at specified values of (T_u, P, ϕ). To maintain adequate resolution of the propagating flame, dynamically adaptive mesh is utilized in simulation and the thin reaction zone is always fully covered by the finest grids [39]. Since 1-D simulation is conducted, the propagating spherical flames are not affected by buoyancy [21] and flame instability [24]. In simulations, the flame front, R_f, is defined as the location of the maximum heat release rate. The spherical flame propagation speed, dR_f/dt, and stretch rate, $K = (2/R_f)(dR_f/dt)$, is calculated through numerical differentiation. As shown in [18], the flame propagation speed and stretch rate are almost independent of the flame front definition.

3. Radiation effects on spherical flame propagation

Our previous study [39] has shown that radiation has two effects on spherical flame propagation: (1) a radiation-induced thermal effect by which flame temperature and thus spherical flame propagation speed are reduced; and (2) a radiation-induced flow effect by which flame propagation speed is reduced due to the inward flow of burned gas generated by radiation cooling. These two effects were further analyzed by Santner et al. [42] by using a simple radiation model and linear approximation of temperature distribution. Though only methane/air flames near the lean flammability limit and at NTP were considered in [39], radiation-induced thermal and flow effects in fact exist in spherical flame experiments of all types of fuel/air mixtures at different conditions. For completeness, the radiation effects on spherical flame propagation and the determination of laminar flame speed are briefly described here. The readers are referred to [39] for more details.

Radiation-induced thermal and flow effects are demonstrated by Figs. 1 and 2. Figure 1 shows the evolution of temperature and flow speed in a rich methane/air spherical flame. Comparison between results from ADI and OTM in Fig. 1(a) shows that the peak flame temperature is reduced after considering radiative loss. Due to radiation, the peak flame temperature is reduced by 15 K and 22 K at t = 20 ms and t = 30 ms, respectively. Due to radiation-induced reduction in flame temperature, the overall reaction rate decreases and so does the flame propagation speed. Figure 1(b) shows that the flow speed of burned gas is zero in the adiabatic case, and that the burned gas moves toward the center when radiative loss is considered. This inward flow is generated by radiation cooling of burned gas as shown in Fig. 1(a) and it slows the spherical flame propagation speed.

In outwardly propagating spherical flame, the stretched flame speed relative to burned gas, S_b, is defined as

$$S_b = dR_f/dt - u_b \tag{1}$$

where dR_f/dt is the propagation speed of the spherical flame front and u_b is the flow speed of burned gas at the end of the reaction

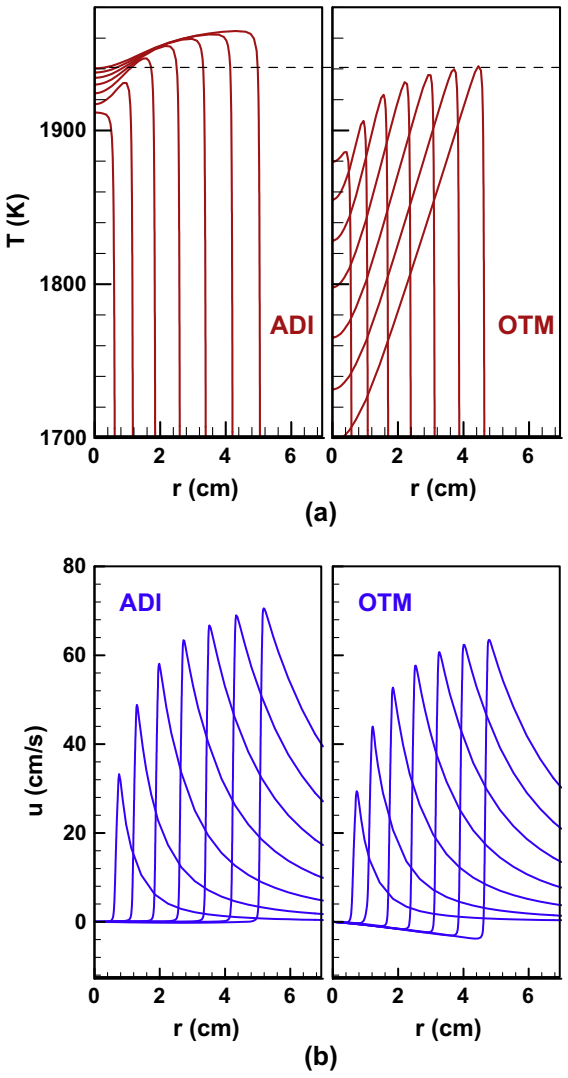

Fig. 1. Distributions of (a) temperature and (b) flow speed for propagating spherical methane/air ($\phi = 1.4$) flames at $T_u = 298$ K and $P = 1$ atm. The distributions are at consecutive equidistant instants of time: $t = 10, 20, 30, 40, 50, 60, 70$ ms.

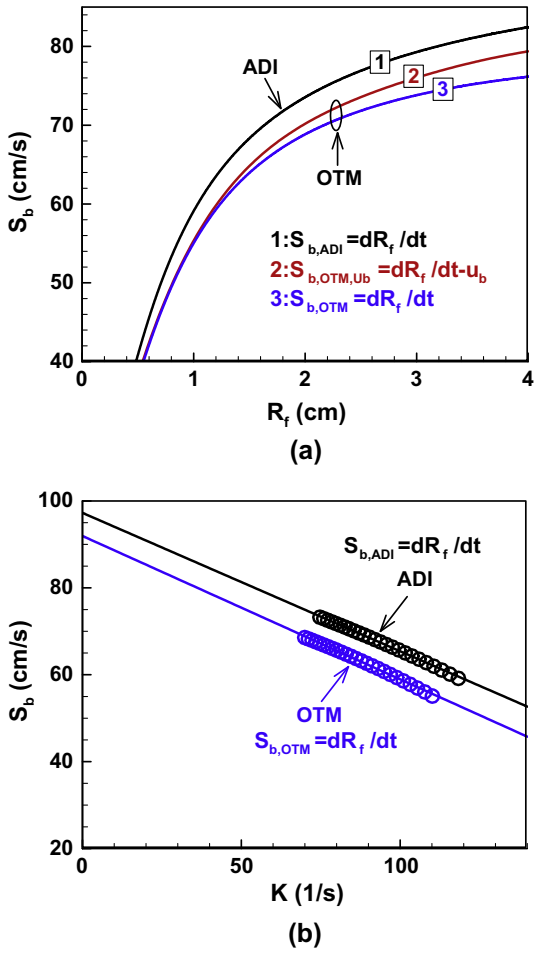

Fig. 2. Change of the flame speed relative to burned gas, S_b, with (a) flame radius, R_f, and (b) stretch rate, K, for spherical methane/air ($\phi = 1.4$) flames at $T_u = 298$ K and $P = 1$ atm. In figure (b), the symbols are data for spherical flames with radii in the range of $1.0 \leqslant R_f \leqslant 2.0$ cm; and the solid lines stand for linear extrapolation according to Eq. (2).

zone after the flame front. Since the burned gas is static in an adiabatic spherical flame (i.e. $u_b = 0$), we have $S_{b,\text{adiabatic}} = dR_f/dt$. When radiation is considered, Fig. 1(b) shows that $u_b < 0$. Therefore, we have $S_{b,\text{radiative}} = dR_f/dt - u_b > dR_f/dt$. In practical spherical flame experiments [6–15], it is difficult to measure u_b and hence the approximation of $S_{b,\text{radiative}} \approx dR_f/dt$ is usually used (i.e. to neglect the inward flow of burned gas by assuming that $u_b \approx 0$). It is noted that the present study only deals with traditional experimental methods [6–15] in which only the flame front speed is measured from high-speed schlieren or shadowgraph. The recent method using direct flow and flame front speed measurements with high-speed PIV [59,60] is not discussed here. Nevertheless, in this case the effect of heat loss through particle radiation and conduction to particles may also affect flame propagation speed.

Figure 2(a) compares flame speeds relative to burned gas for adiabatic and radiative spherical flames predicated by ADI and OTM, respectively. The difference between line 2 ($S_{b,OTM,ub} = dR_f/dt - u_b$) and line 3 ($S_{b,OTM} = dR_f/dt$) is caused by radiation-induced flow effect; and the difference between line 1 ($S_{b,ADI} = dR_f/dt$) and line 2 ($S_{b,OTM,ub} = dR_f/dt - u_b$) is due to radiation-induced thermal effect on S_b. With the increase of flame radius, the magnitude of radiation-induced inward flow increases and so does the value of ($S_{b,OTM,ub} - S_{b,OTM}$). This indicates that flow effect becomes stronger at larger flame radius. According to numerical results shown in Fig. 1(b) and Eq. (7) shown later, the magnitude of radiation-induced inward flow speed at the flame front, $|u_b|$, increases with R_f. Physically, the inward flow is induced by radiation cooling due to mass conservation inside the spherical flame. Radiation cooling reduces the burned gas temperature and increases its density, and thus induces an inward flow. The magnitude of the inward flow speed at the flame front, $|u_b|$, is equal to the ratio between the mass change due to radiation cooling ($\sim R_f^3$) and spherical flame area ($\sim R_f^2$). Therefore, we have $|u_b| \sim R_f$ and hence the radiation-induced flow effect becomes stronger at larger flame radius. On the other hand, ($S_{b,ADI} - S_{b,OTM,ub}$) is shown to be insensitive to the change of R_f. Therefore, radiation-induced thermal effect is nearly independent of spherical flame size when the flame radius is large and the flame stretch is small.

Once the adiabatic, stretched flame speed, S_b, is obtained, the unstretched laminar flame speed, S_b^0, can be extracted from the linear extrapolation based on the following correlation

$$S_b = S_b^0 - L_b K \tag{2}$$

where L_b is Markstein length relative to burned gas and $K = (2/R_f)(dR_f/dt)$ is the stretch rate. As mentioned before, the unstretched laminar flame speed relative to unburned gas, S_u^0, is deduced through mass conservation: $S_u^0 = \sigma S_b^0$. Figure 2(b) shows the linear extrapolation for adiabatic (ADI) and radiative (OTM) cases. Linear

extrapolation of S_b^0 is affected by flame radius range used in data processing as well as radiation (see more details in Section 3.2.1 in [39]). In this study, the data utilized in linear extrapolation of S_b^0 are spherical flames with radii in the range of $1.0 \leqslant R_f \leqslant 2.0$ cm. Figure 2(b) indicates that the linear behavior between S_b and K maintains for both adiabatic (ADI) and radiative (OTM) cases. Theoretically, radiation has a nonlinear effect on flame speeds when the flame temperature is significantly modified for near limit mixtures or when the radiation-induced inward flow is very strong for spherical flames with large radii [39]. In the present study, the modifications to the flame temperature and flame propagation speed caused by, respectively, the radiation-induced thermal and flow effects are very small (both within 3%). This is why a linear model is appropriate for the extrapolation of unstretched flame speed. However, it should be noted that when the mixture is near the flammability limit, the radiation effect on flame speed is nonlinear [29–31,39]. Therefore, care is needed to conduct extrapolation for near limit flames with radiative loss. Fortunately, for most near limit flames, spherical expanding flames are not applicable due to the buoyancy effect [21,37].

Flames with $R_f < 1.0$ cm are not used in data processing due to the effects of ignition energy and unsteady ignition to flame transition [18–20]. Moreover, for very lean and rich propane/air, isooctane/air, and n-heptane/air flames, the flame radius range is changed to $1.5 \leqslant R_f \leqslant 2.0$ cm so that the nonlinear stretch effects due to ignition to flame transition [25–28] can be minimized. It should be noted that spherical flames with $R_f > 2.0$ cm are not used in the present study. This is because in many practical spherical flame experiments with small chamber radius (less than 10 cm) [6–15], data with large flame radii cannot be used due to the influences of pressure rise [22] and/or flame instability [24]. Usually only spherical flames with $R_f \leqslant 2.0$ cm recorded in experiments are used in data processing [6–15]. In fact, since radiation-induced flow effect increases with flame radius, the influence of radiation on laminar flame speed determination might be over-estimated by considering spherical flames at large radii in previous studies by Beeckmann et al. [40] and Egolfopoulos et al. [41]. Moreover, at larger flame radius (e.g., $R_f = 4$ cm), radiation-induced flow becomes stronger and thereby S_b changes nonlinearly with K for radiative cases, which makes the extrapolation of S_b^0 difficult.

It is emphasized that linear extrapolation is used in this study to obtain unstretched laminar flame speed, S_b^0. For mixtures with effective Lewis number significantly different from unity, a nonlinear stretch effect is observed and nonlinear extrapolation should be conducted [18–20]. For all the cases considered in this study, the linear behavior between S_b and K maintains for both adiabatic and radiative cases. Consequently, linear extrapolation can be conducted. Moreover, we compared the results from different linear and nonlinear extrapolations and found that the value radiation-induced uncertainty introduced in the following section is only slightly affected. We also conducted linear extrapolation for spherical flames with other flame radius ranges, $1.0 \leqslant R_f \leqslant 1.5$ cm and $0.7 \leqslant R_f \leqslant 1.5$ cm. Since the radiation-induced flow effect increases with flame radius, the radiation-induced uncertainty is found to increase slightly when spherical flames with larger radii are used in linear extrapolation. Therefore, we can at least provide conservative prediction of radiation-induced uncertainty for experiments using linear extrapolation and smaller flame radii than that in the range of $1.0 \leqslant R_f \leqslant 2.0$ cm.

4. Radiation-induced uncertainty in laminar flame speed measurement

To quantify radiation-induced uncertainty in laminar flame speed measured from propagating spherical flames, we introduce the following variable, R, representing the relative reduction in unstretched laminar flame speed caused by radiation

$$R = 1 - \frac{S^0_{b,\text{radiative}}}{S^0_{b,\text{adiabatic}}} \tag{3}$$

where S_b^0 is the unstretched laminar flame speed relative to burned gas and it is extracted from linear extrapolation between S_b and K according to Eq. (2). In practical spherical flame experiments for laminar flame speed measurement [6–15], usually the flow speed is not measured and it is assumed that $S_b = dR_f/dt$ by neglecting the speed of burned gas. As in experiments, in our simulation we use $S_b = dR_f/dt$ for both adiabatic and radiative cases (i.e. neglecting the inward flow of burned gas). Therefore, radiation-induced thermal and flow effects are both included in R.

For the adiabatic case (ADI), we have $S^0_{u,\text{adiabatic}} = \sigma S^0_{b,\text{adiabatic}}$, where $\sigma = \rho_b/\rho_u$ is the density ratio evaluated at adiabatic equilibrium condition. For radiative cases (OTM or SNB), the density ratio is in fact different from that for the adiabatic case and it is difficult to evaluate. In spherical flame experiments [6–15], the density ratio at adiabatic equilibrium conditions is used for radiative cases to approximate the laminar flame speed relative to unburned gas: $S^0_{u,\text{radiative}} \approx \sigma S^0_{b,\text{radiative}}$. Therefore, from Eq. (3) we have

$$R \approx 1 - \frac{S^0_{u,\text{radiative}}}{S^0_{u,\text{adiabatic}}} \tag{4}$$

In the following, the relative laminar flame speed reduction caused by radiation at NTP is first discussed. Then, results at elevated temperature and pressure are presented.

4.1. Results at normal temperature and pressure

Figure 3 shows the relative laminar flame speed reduction as a function of equivalence ratio for three hydrocarbon fuels (CH_4, C_3H_8, and iC_8H_{18}) at NTP. It is observed that R reaches a minimum value when the equivalence ratio is around 1.1, and that R has larger value when the mixture becomes leaner or richer. This is reasonable since radiation effects become stronger when the lean or rich flammability limit is approached [39]. Moreover, Fig. 3 shows that R predicted by SNB is slightly lower than that by OTM. This is due to the fact that radiation-induced thermal and flow effects are both reduced when radiation (re)absorption is considered [39]. Since SNB is more accurate than OTM [30,37], R predicted by SNB should be used to quantify radiation-induced laminar flame speed reduction or uncertainty in practical spherical flame experiments. Except in Figs. 3 and 5, in all other figures R is predicted by SNB.

By plotting R for different fuels (CH_4, C_3H_8, and iC_8H_{18}) as a function of ϕ, we find that R depends on fuel as well as ϕ. Therefore, there is no simple correlation between R and ϕ. Instead of R versus ϕ, in Fig. 4 we plot R versus the adiabatic laminar flame speed, $S^0_{u,\text{ADI}}$, normalized by $S_0 = 1$ cm/s. Luckily, it is observed that R monotonically decreases with $S^0_{u,\text{ADI}}/S_0$ and that this change is nearly fuel-independent. Therefore, relative laminar flame speed reduction caused by radiation can be fuel-independently determined by the adiabatic laminar flame speed, i.e. $R = R\left(S^0_{u,\text{ADI}}\right)$. This is reasonable since the radiating time of burned gas is determined by flame propagation speed (which is equal to $S^0_{u,\text{ADI}}/\sigma$ in zeroth-order approximation) for spherical flames within specified flame radius range. Figure 4 shows that the relative laminar flame speed reduction caused by radiation is less than 5% for $S^0_{u,\text{ADI}} \geqslant 12$ cm/s and within 2% for $S^0_{u,\text{ADI}} \geqslant 26$ cm/s. Therefore, the present results demonstrate that at NTP, radiation-induced uncertainty/reduction

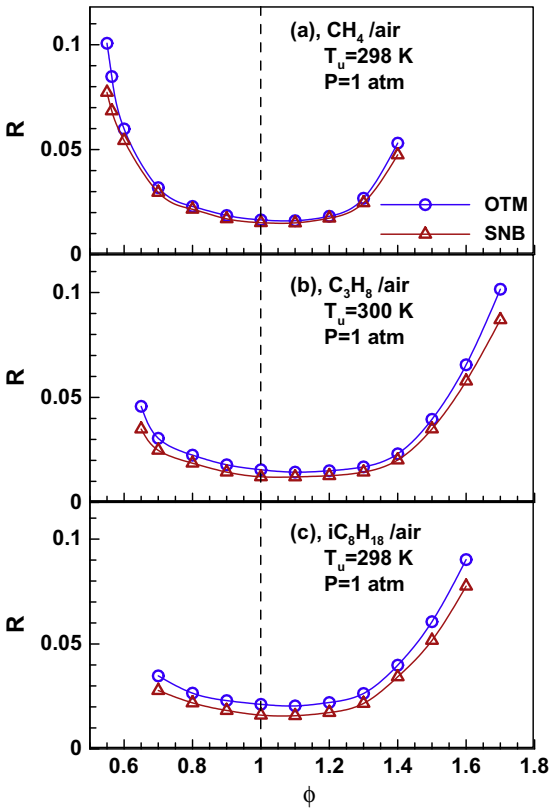

Fig. 3. Relative laminar flame speed reduction caused by radiation for (a) CH_4/air, (b) C_3H_8/air, and (c) iC_8H_{18}/air mixtures at NTP.

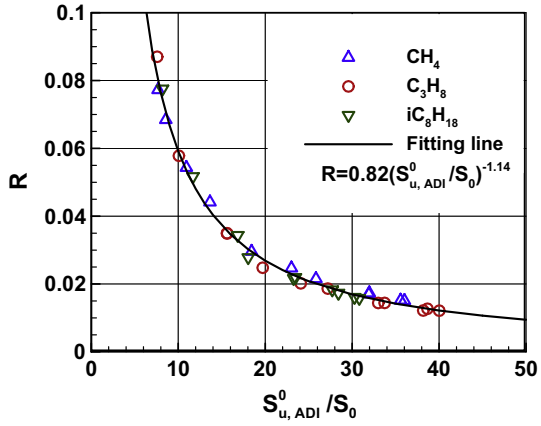

Fig. 4. Relative laminar flame speed reduction, R, as a function of normalized laminar flame speed, $S^0_{u,ADI}/S_0$ (where $S_0 = 1$ cm/s), for different fuel/air mixtures at NTP (Nos. 1–3 in Table 2).

in laminar flame speed measured from propagating spherical flames is within 5% and 2% for mixtures with laminar flame speed above 12 cm/s and 26 cm/s, respectively.

The results in Fig. 4 can be empirically correlated by the following relationship

$$R = 0.82\left(\frac{S^0_{u,\mathrm{ADI}}}{S_0}\right)^{-1.14} \tag{5}$$

in which $S_0 = 1$ cm/s and two coefficients (0.82 and −1.14) are obtained from fitting. Eq. (5) might be used to predict radiation-induced uncertainty/reduction in laminar flame speed measured from propagating spherical flames for hydrocarbon/air mixtures at NTP.

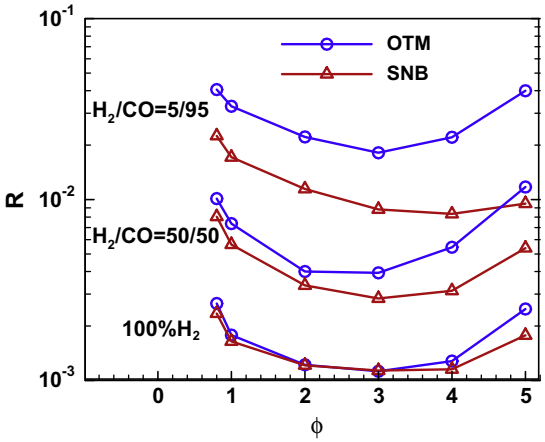

Fig. 5. Relative laminar flame speed reduction for syngas/air and hydrogen/air mixtures at $T_u = 298$ K and $P = 1$ atm.

Besides hydrocarbon fuels, we also study propagating spherical flames for syngas (including pure hydrogen), DME, and n-heptane at NTP (Nos. 4–10 in Table 2). Some results for syngas are presented in Fig. 5. It is observed that for pure H_2 and H_2/CO(=50/50), the relative laminar flame speed reduction caused by radiation is within 1%. These mixtures have high laminar flame speed (above 50 cm/s) and thereby radiation-induced reduction in laminar flame speed measured from propagating spherical flame is very small. Moreover, Fig. 5 shows that the difference between R predicted by SNB and that by OTM becomes larger for richer syngas/air mixtures with lower H_2/CO ratio. This is due to radiation (re)absorption caused by large amount of CO in the mixture.

In Fig. 6 we plot the results (predicted by SNB) for syngas and hydrocarbon fuels at NTP (Nos. 1–8 in Table 2) as well as the prediction by in Eq. (5). It is seen that the empirical correlation works fairly well for syngas/air and hydrogen/air mixtures at NTP. Moreover, Fig. 7 shows that the empirical correlation works very well for DME/air and n-heptane at NTP. The empirical correlation, Eq. (5), is obtained based on results for CH_4, C_3H_8, and iC_8H_{18}, and Figs. 6 and 7 shows that it works for H_2/CO, DME, and n-Heptane. The disadvantages of this correlation are that it is "empirical" and not as rigorous as an "analytical" one and that it has not been tested for all different fuels. Nevertheless, it is expected that Eq. (5) can be used to quantify radiation-induced uncertainty/reduc-

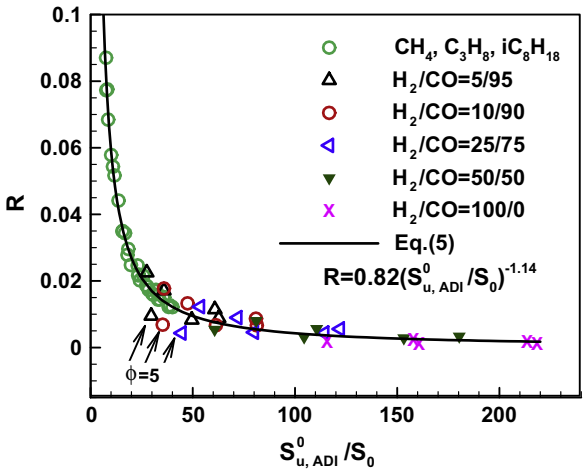

Fig. 6. R versus $S^0_{u,ADI}/S_0$ for different fuel/air mixtures at NTP (Nos. 1–8 in table 2).

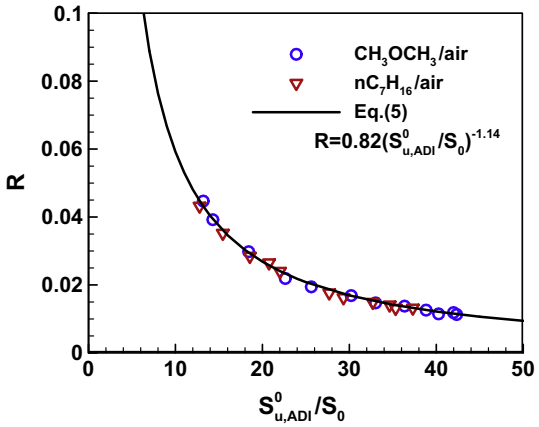

Fig. 7. R versus $S^0_{u,ADI}/S_0$ for DME/air and nC_7H_{16}/air mixtures at $T_u = 298$ K and $P = 1$ atm (Nos. 9 and 10 in Table 2).

tion in laminar flame speed measured from propagating spherical flames for fuel/air mixtures at NTP. It is emphasized that there is uncertainty in the empirical correlation given in Eq. (5) and that the prediction by Eq. (5) is not exact the same as that from simulation of adiabatic and radiative spherical flames (see Figs. 4, 6 and 7). Besides, as mentioned in the last paragraph in Section 3, the value of R is slightly affected by the linear/nonlinear model and flame radius range used in extrapolation. The uncertainty in the above empirical correlation for R is estimated to be ±0.005. It is noted that in spherical flame experiments the radiative laminar flame speed, $S^0_{u,Exp} \approx S^0_{u,SNB}$, rather than the adiabatic one, $S^0_{u,ADI}$, is measured. The empirical correlation in Eq. (5) can be used in first-order approximation by simply replacing $S^0_{u,ADI}$ with $S^0_{u,Exp}$.

Furthermore, it should be emphasized that the empirical correlation in Eq. (5) works only for fuel/air mixtures without dilution (especially CO_2/H_2O with strong radiation reabsorption). We also conduct simulations for propagating spherical flames of stoichiometric CH_4/air mixtures with different amounts of CO_2 dilution (the volumetric fraction of CO_2 in CH_4/air/CO_2 mixture changes from 0% to 20%) at NTP. Figure 8 shows that Eq. (5) over-predicts radiation-induced relative laminar flame speed reduction for CH_4/air with CO_2 dilution. This is because CO_2 is not only a radiation emitter but also an absorber. When there is large amount of CO_2 in the unburned fuel/air mixture, radiative heat loss from the burned gas can be reabsorbed by CO_2 in the unburned mixture which makes the flame stronger and thereby increases the laminar flame speed [30,31,37]. As a result, radiation-induced uncertainty in fact

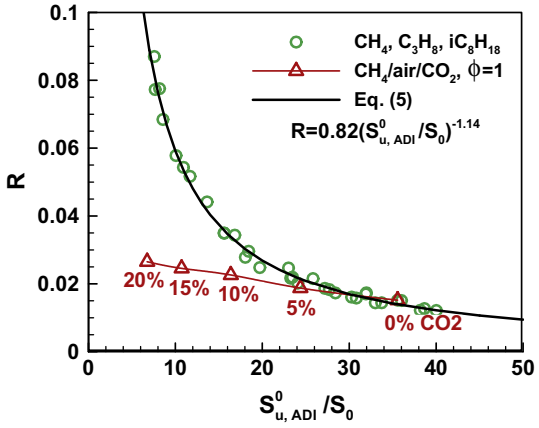

Fig. 8. R versus $S^0_{u,ADI}/S_0$ for different fuel/air mixtures (Nos. 1–3 in Table 2) and stoichiometric CH_4/air with different amounts of/CO_2 dilutions at NTP.

decreases when the fuel/air mixture is diluted by species with strong radiation reabsorption. It is noticed that in Fig. 6, the empirical correlation has slight over-prediction for syngas/air mixtures (H_2/CO = 5/95, 10/90, and 25/75) at $\phi = 5.0$, which contain a large amount of CO with strong radiation reabsorption.

4.2. Results at elevated temperature

To quantify radiation-induced uncertainty in laminar flame speed measured at elevated temperature, we study the spherical flames of CH_4/air and iC_8H_{18}/air mixtures at elevated temperature and atmospheric pressure (Nos. 11–14 in Table 2, Figs. 9 and 10).

Figure 9(a) shows that when the equivalence ratio is fixed, R decreases with increasing initial temperature, T_u. On the other hand, Fig. 9(b) shows that when the laminar flame speed is fixed, R increases with increasing T_u. These observations can be explained with the help of Eq. (4). Since burned gas temperature increases with T_u, radiation-induced thermal and flow effects both increase with T_u and thereby the difference, $S^0_{u,adiabatic} - S^0_{u,radiative}$, increases with T_u. When the laminar flame speed, $S^0_{u,adiabatic}$, is fixed, the definition in Eq. (3) indicates that R should increase with T_u. When the equivalence ratio is fixed, $S^0_{u,adiabatic}$ increases with T_u at much faster speed than $S^0_{u,adiabatic} - S^0_{u,radiative}$ does. Therefore, Eq. (4) indicates that R should decrease with T_u at fixed equivalence ratio.

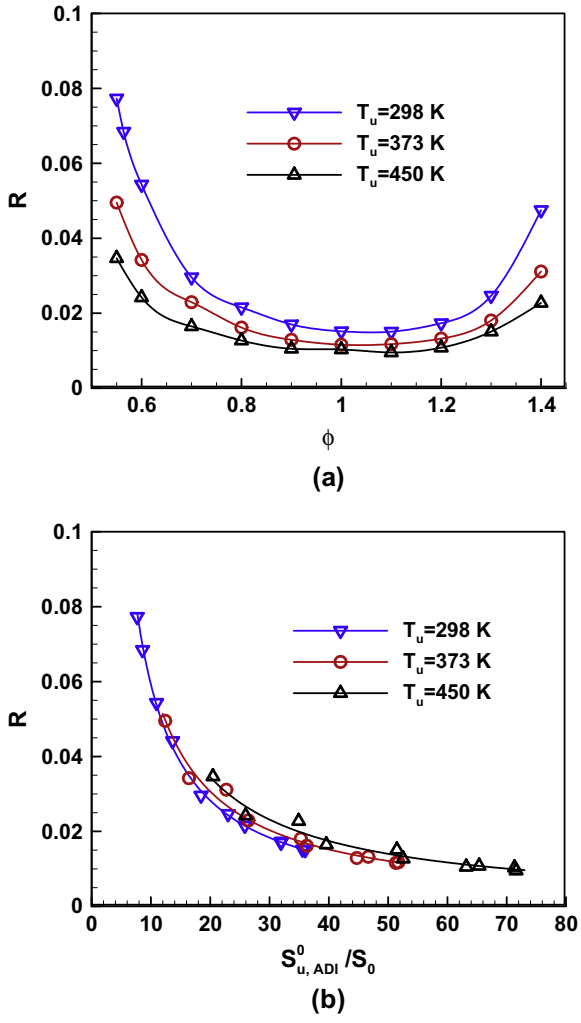

Fig. 9. Relative laminar flame speed reduction at different initial temperatures for CH_4/air at $P = 1$ atm.

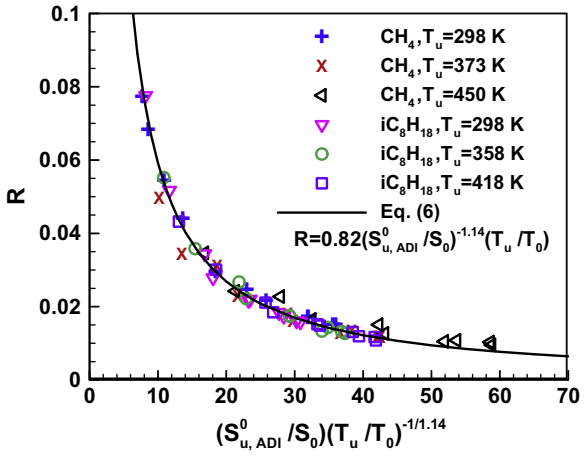

Fig. 10. R versus $\left(S^0_{u,\mathrm{ADI}}/S_0\right)(T_u/T_0)^{-1/1.14}$ for CH_4/air (P = 1 atm) and iC_8H_{18}/air (P = 0.1 MPa) at different initial temperatures (Nos. 1, 3, 11∼14 in Table 2). S_0 = 1 cm/s, T_0 = 298 K.

Since Fig. 9(b) demonstrates that R depends on T_u as well as $S^0_{u,\mathrm{ADI}}$, the correlation in Eq. (5) cannot be used to predict radiation-induced uncertainty/reduction at elevated temperature. To include the influence of initial temperature, T_u, various possible empirical correlations for $R = R\left(S^0_{u,\mathrm{ADI}}, T_u\right)$ are studied. The following correlation is eventually chosen after considering the accuracy and simplicity:

$$R = 0.82\left(\frac{S^0_{u,\mathrm{ADI}}}{S_0}\right)^{-1.14}\left(\frac{T_u}{T_0}\right) \tag{6}$$

where S_0 = 1 cm/s and T_0 = 298 K. The temperature term in Eq. (6) is due to the fact that radiation intensity increases with temperature. As mentioned before, radiation-induced thermal and flow effects both increase with T_u and thereby R also increases with T_u. It is noted that the temperature term in Eq. (6) is not raised to the fourth power. To ensure the same adiabatic laminar flame speed at higher initial temperature, the mixture must be leaner or richer such that the adiabatic flame temperature and burned gas temperature in fact become lower. Therefore, the radiative loss and R do not scale with T_u to the fourth power when the adiabatic laminar flame speed is fixed. However, it is difficult to explain why R changes linearly with T_u.

In Fig. 10 the results of for different CH_4/air and iC_8H_{18}/air mixtures at different initial temperatures (corresponding to Nos. 1, 3, 11–14 in Table 2) are indicated by the symbols and Eq. (6) by the solid line. It is seen that R from the empirical correlation in Eq. (6) agrees well with those from detailed simulations. Therefore, Eq. (6) can be used to quantify radiation-induced uncertainty/reduction in laminar flame speed measured from propagating spherical flames for different fuel/air mixtures at normal and elevated temperatures and atmospheric pressure.

4.3. Results at elevated pressure

The results discussed above are only for fuel/air mixtures at atmospheric pressure. To quantify radiation-induced uncertainty in laminar flame speed measured at elevated pressure, we study the spherical flames of CH_4/air and iC_8H_{18}/air mixtures at different pressures up to 12 atm (Nos. 15–21 in Table 2, Figs. 11 and 12).

Figure 11(a) shows that the change of R with ϕ at elevated pressure is similar to that at atmospheric pressure: R becomes minimum when ϕ is close to 1.0 or 1.1; and R reaches the maximum value when ϕ is close to the lean or rich flammability limit.

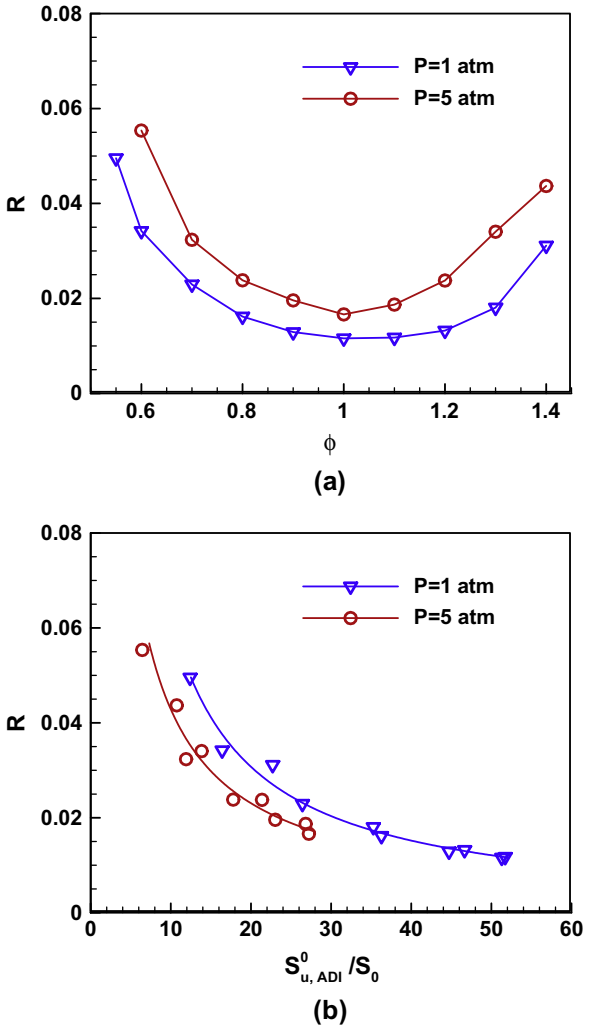

Fig. 11. Relative laminar flame speed reduction at different pressures for CH_4/air at T_u = 373 K.

Moreover, Fig. 11(a) demonstrates that for the same equivalence ratio, R increases with pressure P. This is mainly due to the fact that laminar flame speed decreases with pressure so the burned gas has longer radiating time at higher pressure.

Figure 11(b) shows that the change of R with $S^0_{u,\mathrm{ADI}}/S_0$ at elevated pressure is similar to that at atmospheric pressure. Therefore, the empirical correlation in Eq. (6) can be extended by properly scaling the pressure effects. Furthermore, it is observed that when the laminar flame speed is fixed, R decreases with P. This is counter-intuitive since the influence of radiation is usually considered to increase with pressure (e.g., [42]). The following expression for radiation-induced inward flow, u_b, can be derived from conservation equations for burned gas inside the spherical flame

$$u_b = -\left(1-\frac{1}{\gamma}\right)\frac{1}{R_f^2 P}\int_0^{R_f} r^2 q_r(T, C_K)dr \tag{7}$$

where γ is the heat capacity ratio. In Eq. (7), q_r is the radiative loss which is a function of temperature, T, and molar concentration of different species, C_K, of burned gas inside the spherical flame. With the increase of pressure, the radiative loss increases and so does the integration in Eq. (7). However, the magnitude of radiation-induced inward flow, $|u_b|$, in fact decreases with pressure. This is due to the appearance of pressure in the denominator (since the mass flux across the spherical flame front is equal to $4\pi\rho u_b R_f^2$ and density is proportional to pressure, there is a pressure term in the denomina-

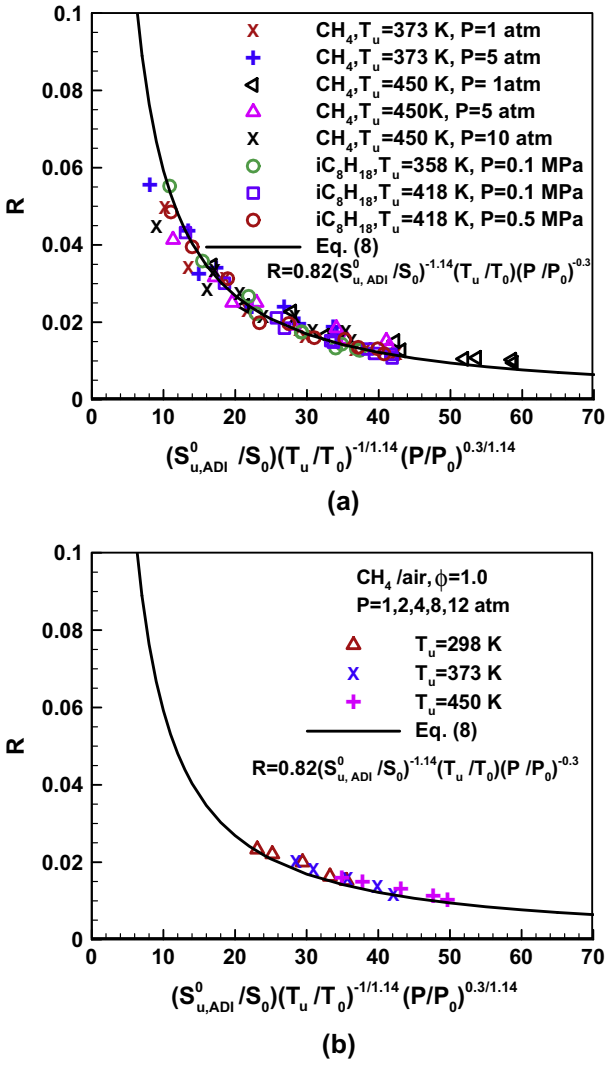

Fig. 12. R versus $\left(S^0_{u,\mathrm{ADI}}/S_0\right)(T_u/T_0)^{-1/1.14}(P/P_0)^{0.3/1.14}$ for CH_4/air and iC_8H_{18}/air at different initial temperatures and pressures: (a), Nos. 11–18; (b), Nos. 19–21 in Table 2. S_0 = 1 cm/s, T_0 = 298 K, P_0 = 1 atm.

tor of Eq. (7). This conclusion is confirmed by transient 1-D simulation with detailed chemistry and transport via A-SURF. Therefore, the radiation-induced flow effect in fact decreases with pressure, which makes R decrease with P for fixed laminar flame speed.

According to the above discussions, radiation-induced uncertainty/reduction in laminar flame speed measured from propagating spherical flames, R, is affected in the opposite ways by the initial temperature, T_u, and pressure, P. When the equivalence ratio is fixed, R decreases with T_u but increases with P. When the laminar flame speed is fixed, R increases with T_u but decreases with P.

As mentioned before, the empirical correlation in Eq. (6) can be extended by properly scaling the pressure effects. The following empirical correlation is proposed to quantify radiation-induced uncertainty/reduction in laminar flame speed measured at normal and elevated temperatures and pressures:

$$R = 0.82\left(\frac{S^0_{u,\mathrm{ADI}}}{S_0}\right)^{-1.14}\left(\frac{T_u}{T_0}\right)\left(\frac{P}{P_0}\right)^{-0.3} \tag{8}$$

where S_0 = 1 cm/s, T_0 = 298 K, and P_0 = 1 atm. It is noted that $S^0_{u,\mathrm{ADI}}$ is evaluated at T_u and P, not at T_0 and P_0. The results for different CH_4/air and iC_8H_{18}/air mixtures at elevated pressures (corresponding to Nos. 15∼21 in Table 2) are plotted in Fig. 12. Slight over-prediction by Eq. (8) is observed for mixtures with very low laminar flame speed (below 15 cm/s and thus might be affected by buoyancy in practical experiments). Nevertheless, the empirical correlation in Eq. (8) gives good evaluation of the relative laminar flame speed reduction, R. Therefore, Eq. (8) can be used to quantify radiation-induced uncertainty/reduction in laminar flame speed measured from propagating spherical flames for different fuel/air mixtures at normal and elevated temperatures and pressures. Compared to the correlation given by Eq. (5) for normal temperature and pressure, the above empirical correlation for R at elevated temperatures and pressures has larger uncertainty, which is estimated to around ±0.01 for $S^0_{u,\mathrm{ADI}} \geqslant 12$ cm/s. Again, the laminar flame speed measured in spherical flame experiments, $S^0_{u,\mathrm{Exp}}$, can be used to replace $S^0_{u,\mathrm{ADI}}$ in Eq. (8) to get radiation-induced uncertainty in first-order approximation.

It should be noted we cannot explain the specific values of power exponents in the empirical correlation in Eq. (8). These exponents are obtained from fitting the data into power law. As mentioned before, the radiating time of burned gas is determined by flame propagation speed and thereby R should decrease with the increase of $S^0_{u,\mathrm{ADI}}$, indicating the power exponent for $S^0_{u,\mathrm{ADI}}$ is negative. For the same flame speed, T_u increases the flame temperature and thus the radiation heat loss, indicating positive power exponent for T_u. For the same flame speed and temperature, the increase of pressure reduces the radiation-induced flow effect (see Eq. (7) and related discussions). Therefore, the power exponent for P is negative.

5. Radiation-corrected flame speed (RCFS)

Since the empirical correlation in Eq. (8) can quantify radiation-induced reduction in laminar flame speed, we can make use of Eq. (8) to get the RCFS. According to the definition in Eq. (4) and the empirical correlation in Eq. (8), we have the following expression for the difference between adiabatic (ADI) and radiative (SNB) laminar flame speed

$$S^0_{u,\mathrm{ADI}} - S^0_{u,\mathrm{SNB}} = 0.82 S^0_{u,\mathrm{ADI}}\left(\frac{S^0_{u,\mathrm{ADI}}}{S_0}\right)^{-1.14}\left(\frac{T_u}{T_0}\right)\left(\frac{P}{P_0}\right)^{-0.3} \tag{9}$$

The laminar flame speed measured in practical experiments, $S^0_{u,\mathrm{Exp}}$, is close to the radiative one, i.e. $S^0_{u,\mathrm{Exp}} \approx S^0_{u,\mathrm{SNB}}$. And the RCFS is equal to the adiabatic one, $S^0_{u,\mathrm{RCFS}} = S^0_{u,\mathrm{ADI}}$. From Eq. (9) we have the following implicit expression for the RCFS, $S^0_{u,\mathrm{RCFS}}$,

$$S^0_{u,\mathrm{RCFS}} = S^0_{u,\mathrm{Exp}} + 0.82 S^0_{u,\mathrm{RCFS}}\left(\frac{S^0_{u,\mathrm{RCFS}}}{S_0}\right)^{-1.14}\left(\frac{T_u}{T_0}\right)\left(\frac{P}{P_0}\right)^{-0.3} \tag{10}$$

Once the laminar flame speed, $S^0_{u,\mathrm{Exp}}$, at T_u and P is obtained using the propagating spherical flame method, we can get the RCFS, $S^0_{u,\mathrm{RCFS}}$, by solving Eq. (10) numerically using the Newton iteration method. In first-order approximation, we have

$$S^0_{u,\mathrm{RCFS}} = S^0_{u,\mathrm{Exp}} + 0.82 S^0_{u,\mathrm{Exp}}\left(\frac{S^0_{u,\mathrm{Exp}}}{S_0}\right)^{-1.14}\left(\frac{T_u}{T_0}\right)\left(\frac{P}{P_0}\right)^{-0.3} \tag{11}$$

in which the last term is the radiation-correction term. The RCFS obtained using the method proposed here can be directly compared with the laminar flame speed predicted by kinetic models during the chemistry validation and optimization process.

6. Conclusions

Numerical simulations with detailed chemistry and transport are conducted for propagating spherical flames of different

fuel/air mixtures at normal and elevated temperatures and pressures. The radiative effects are conservatively evaluated without considering wall-reflected radiation. Effects of radiation on spherical flame propagation are discussed and the radiation-induced uncertainty/reduction in laminar flame speed measurement using propagating spherical flames is quantified. The main conclusions are:

1. Radiation-induced reduction in laminar flame speed, R, can be fuel-independently determined by the adiabatic laminar flame speed. An empirical correlation, $R = 0.82\left(S^0_{u,\mathrm{ADI}}/S_0\right)^{-1.14}$, is obtained to predict radiation-induced uncertainty/reduction in laminar flame speed measured from propagating spherical flames for fuel/air mixtures at NTP. Radiation-induced uncertainty/reduction at NTP is within 5% and 2% for mixtures with laminar flame speed above 12 cm/s and 26 cm/s, respectively. This indicates that the laminar flame speed is reduced by about 0.6 cm/s due to radiation. This amount of change in laminar flame speed might be much smaller than the change caused by other factors which influence the accuracy in laminar flame speed measurement.
2. R is affected in the opposite ways by the initial temperature, T_u, and pressure, P. When the equivalence ratio is fixed, R decreases with T_u but increases with P. However, when the laminar flame speed is fixed, R increases with T_u but decreases with P.
3. An empirical correlation, $R = 0.82\left(S^0_{u,\mathrm{ADI}}/S_0\right)^{-1.14}(T_u/T_0)(P/P_0)^{-0.3}$ with $S_0 = 1$ cm/s, $T_0 = 298$ K, and $P_0 = 1$ atm, is proposed to quantify radiation-induced uncertainty/reduction in laminar flame speed measured from propagating spherical flames for fuel/air mixtures at normal and elevated temperatures and pressures. This correlation can be directly used in spherical flame experiments by simply replacing $S^0_{u,\mathrm{ADI}}$ with $S^0_{u,\mathrm{Exp}}$.
4. Once the flame speed, $S^0_{u,\mathrm{Exp}}$, is measured using propagating spherical flames at T_u and P, we can get the radiation-corrected flame speed (RCFS) according to Eq. (10).

It is emphasized again that the empirical correlation and RCFS do NOT work for fuel/air mixtures diluted by CO_2 or H_2O which has strong radiation reabsorption. Radiation reabsorption is shown to reduce the value of R. The radiation-induced uncertainty/reduction for this type of mixtures deserves further investigation.

Acknowledgments

This work was supported by National Natural Science Foundation of China (Nos. 51322602 and 51136005), US Department of Energy, Office of Basic Energy Sciences as part of an Energy Frontier Research Center on Combustion with Grant No. DESC0001198, and National Research Foundation of Korea (MEST, No. 2013-023030). Z.C. also thanks the support from State Key Laboratory of Engines at Tianjin University (No. K2014-01) and Key Laboratory of Low-grade Energy Utilization Technologies and Systems at Chongqing University (No. LLEUTS 201304).

References

[1] C.K. Law, C.J. Sung, H. Wang, T.F. Lu, AIAA J. 41 (2003) 1629–1646.
[2] E. Ranzi, A. Frassoldati, R. Grana, A. Cuoci, T. Faravelli, A.P. Kelley, C.K. Law, Prog. Energy Combust. Sci. 38 (2012) 468–501.
[3] S. Dooley, S.H. Won, M. Chaos, et al., Combust. Flame 157 (2010) 2333–2339.
[4] M.P. Burke, M. Chaos, Y. Ju, F.L. Dryer, S.J. Klippenstein, Int. J. Chem. Kinet. 44 (2012) 444–474.
[5] J. Santner, F.L. Dryer, Y.G. Ju, Proc. Combust. Inst. 34 (2013) 719–726.
[6] S.C. Taylor. Burning velocity and the influence of flame stretch. Ph.D. Thesis, University of Leeds, 1991.
[7] L.K. Tseng, M.A. Ismail, G.M. Faeth, Combust. Flame 95 (1993) 410–426.
[8] D. Bradley, R.A. Hicks, M. Lawes, C.G.W. Sheppard, R. Woolley, Combust. Flame 115 (1998) 126–144.
[9] S.D. Tse, D.L. Zhu, C.K. Law, Proc. Combust. Inst. 28 (2000) 1793–1800.
[10] X. Qin, Y. Ju, Proc. Combust. Inst. 30 (2005) 233–240.
[11] Z. Huang, Y. Zhang, K. Zeng, B. Liu, Q. Wang, D.M. Jiang, Combust. Flame 146 (2006) 302–311.
[12] Z. Chen, X. Qin, Y.G. Ju, Z.W. Zhao, M. Chaos, F.L. Dryer, Proc. Combust. Inst. 31 (2007) 1215–1222.
[13] T. Tahtouh, F. Halter, C. Mounaïm-Rousselle, Combust. Flame 156 (2009) 1735–1743.
[14] W.B. Lowry, Z. Serinyel, M.C. Krejci, H.J. Curran, G. Bourque, E.L. Petersen, Proc. Combust. Inst. 33 (2011) 929–937.
[15] J. Beeckmann, L. Cai, H. Pitsch, Fuel 117 (2014) 340–350.
[16] J.T. Farrell, R.J. Johnston, I.P. Androulakis, SAE 2004-01-2936.
[17] Z. Chen, Int. J. Hydrogen Energy 34 (2009) 6558–6567.
[18] D. Bradley, P.H. Gaskell, X.J. Gu, Combust. Flame 104 (1996) 176–198.
[19] Z. Chen, M.P. Burke, Y. Ju, Proc. Combust. Inst. 32 (2009) 1253–1260.
[20] H.H. Kim, S.H. Won, J.S. Santner, Z. Chen, Y. Ju, Proc. Combust. Inst. 34 (2013) 929–936.
[21] L. Qiao, Y.X. Gu, W.J.A. Dam, E.S. Oran, G.M. Faeth, Proc. Combust. Inst. 31 (2007) 2701–2709.
[22] Z. Chen, M.P. Burke, Y. Ju, Combust. Theory Model. 13 (2009) 343–364.
[23] M.P. Burke, Z. Chen, Y. Ju, F.L. Dryer, Combust. Flame 156 (2009) 771–779.
[24] D. Bradley, M. Lawes, K. Liu, S. Verhelst, R. Woolley, Combust. Flame 149 (2007) 162–172.
[25] A.P. Kelley, C.K. Law, Combust. Flame 156 (2009) 1844–1851.
[26] F. Halter, T. Tahtouh, C. Mounaïm-Rousselle, Combust. Flame 157 (2010) 1825–1832.
[27] Z. Chen, Combust. Flame 158 (2011) 291–300.
[28] F. Wu, W. Liang, Z. Chen, Y. Ju, C.K. Law, Uncertainty in stretch extrapolation of laminar flame speed from expanding spherical flames. Submitted to 35th Symposium on Combustion. Accepted for oral presentation (2014).
[29] Y. Ju, H.S. Guo, K. Maruta, F.S. Liu, J. Fluid Mech. 342 (1997) 315–334.
[30] Y. Ju, G. Masuya, P.D. Ronney, Proc. Combust. Inst. 27 (1998) 2619–2626.
[31] Y. Ju, H.S. Guo, F.S. Liu, K. Maruta, J. Fluid Mech. 379 (1999) 165–190.
[32] P.D. Ronney, G.I. Sivashinsky, SIAM J. Appl. Math. 49 (1989) 1029–1046.
[33] J.K. Bechtold, C. Cui, M. Matalon, Proc. Combust. Inst. 30 (2005) 177–184.
[34] Z. Chen, Y. Ju, Combust. Theory Model. 11 (2007) 427–453.
[35] Z. Chen, X. Gou, Y. Ju, Combust. Sci. Technol. 182 (2010) 124–142.
[36] I.C. McLean, D.B. Smith, S.C. Taylor, Proc. Combust. Inst. 25 (1994) 749–757.
[37] Z. Chen, X. Qin, B. Xu, Y.G. Ju, F.S. Liu, Proc. Combust. Inst. 31 (2007) 2693–2700.
[38] L. Qiao, Y. Gan, T. Nishiie, W.J.A. Dam, E.S. Oran, Combust. Flame 157 (2010) 1446–1455.
[39] Z. Chen, Combust. Flame 157 (2010) 2267–2276.
[40] J. Beeckmann, N. Chaumeix, P. Dagaut, et al., Collaborative study for accurate measurements of laminar burning velocity, in: Proceedings of the European Combustion Meeting, Lund, Sweden, 2013, pp. P3–P76.
[41] J. Jayachandran, R. Zhao, F.N. Egolfopoulos, Combust. Flame 161 (2014) 2305–2316.
[42] J. Santner, F.M. Haas, Y.G. Ju, F.L. Dryer, Combust. Flame 161 (2014) 147–153.
[43] F. Liu, O. Gulder, G. Smallwood, Int. J. Heat Mass Transfer 41 (1998) 2227–2236.
[44] D.A. Sheen, H. Wang, Combust. Flame 158 (2011) 2358–2374.
[45] X. You, T. Russi, A. Packard, M. Frenklach, Proc. Combust. Inst. 33 (2011) 509–516.
[46] R.J. Kee, F.M. Rupley, J.A. Miller, Sandia National Laboratory, Report SAND89-8009B, 1989.
[47] Z. Chen, M.P. Burke, Y. Ju, Proc. Combust. Inst. 33 (2011) 1219–1226.
[48] H. Zhang, Z. Chen, Combust. Flame 158 (2011) 1520–1531.
[49] W.K. Zhang, Z. Chen, W.J. Kong, Combust. Flame 159 (2012) 151–160.
[50] H. Zhang, P. Guo, Z. Chen, Proc. Combust. Inst. 34 (2013) 3267–3275.
[51] W. Liang, Z. Chen, F. Yang, H. Zhang, Proc. Combust. Inst. 34 (2013) 695–702.
[52] G.P. Smith, D.M. Golden, M. Frenklach, et al., <http://www.me.berkeley.edu/gri_mech/>.
[53] Z.W. Qin, V.V. Lissianski, H.X. Yang, W.C. Gardiner, S.G. Davis, H. Wang, Proc. Combust. Inst. 28 (2000) 1663–1669.
[54] M. Chaos, A. Kazakov, Z. Zhao, F.L. Dryer, Int. J. Chem. Kinet. 39 (2007) 399–414.
[55] S.G. Davis, A.V. Joshi, H. Wang, F. Egolfopoulos, Proc. Combust. Inst. 30 (2005) 1283–1292.
[56] Z. Zhao, M. Chaos, A. Kazakov, F.L. Dryer, Int. J. Chem. Kinet. 40 (2008) 1–18.
[57] X.L. Gou, W.T. Sun, Z. Chen, Y.G. Ju, Combust. Flame 157 (2010) 1111–1121.
[58] X.L. Gou, Z. Chen, W.T. Sun, Y.G. Ju, Combust. Flame 160 (2013) 225–231.
[59] S. Balusamy, A. Cessou, B. Lecordier, Exp. Fluids 50 (2011) 1109–1121.
[60] E. Varea, V. Modica, A. Vandel, B. Renou, Combust. Flame 159 (2012) 577–590.